Physica B 629 (2022) 413654

Contents lists available at ScienceDirect

Physica B: Physics of Condensed Matter

journal homepage: www.elsevier.com/locate/physb

Tailoring the microwave properties of thin Permalloy films using a periodically grooved substrate

A.V. Izotov [a,b,*], B.A. Belyaev [a,b], N.M. Boev [a,b], A.V. Burmitskikh [a,b], A.A. Leksikov [b], G. V. Skomorokhov [b], P.N. Solovev [b,**]

[a] Siberian Federal University, 79 Svobodny pr., 660041, Krasnoyarsk, Russia
[b] Kirensky Institute of Physics, Federal Research Center KSC SB RAS, 50/38 Akademgorodok, 660036, Krasnoyarsk, Russia

ARTICLE INFO

Keywords:
Patterned film
Topography-induced anisotropy
Netzelmann approach
Ferromagnetic resonance
Damping parameter

ABSTRACT

Thin magnetic films with periodic surface topography are of special interest for microwave applications as their static and dynamic magnetic characteristics can be readily adjusted. In this paper, we explore the capabilities of a simple method for producing large-area periodically patterned films by creating regularly spaced grooves on a substrate using a diamond cutter. For 110-nm-thick films, it was found that the substrate-topography-induced magnetic anisotropy was inversely proportional to the pattern period, which in experimental samples varied from 5 to 20 μm. Based on the Netzelmann theory, analytical expressions for demagnetization tensor components were obtained, which accord well with the experimental data. The measurements of the natural ferromagnetic resonance spectra demonstrated that the increase of the topography-induced magnetic anisotropy with the decrease of the pattern period led to the increase of the resonance frequency from 0.65 to 1.86 GHz, and to a decrease of the linewidth and effective damping parameter.

1. Introduction

The rapid development of telecommunication and information technologies led to the widespread usage of microwave electronic devices, from usual read-write heads in hard drive disks to modern navigation satellite, radar and communication systems. The increase in the operating speed of the devices, the bandwidth of communication channels, and the amount of processed data [1] while meeting modern requirements for miniaturization and integration of electronic components is a challenging task. This cannot be accomplished without the utilization of magnetic materials with specified microwave properties (high magnetic permeability and low losses) [2].

The frequency of natural ferromagnetic resonance (NFMR), observed at zero applied magnetic field, usually determines the limiting operating frequency of microwave devices. Both the NFMR frequency and the magnetic permeability depend in a complicated way on material composition, its micromagnetic and crystalline structures, and on specifics of the material fabrication and processing [3]. However, for most bulk magnetic materials, the relation between the NFMR frequency and the magnetic permeability follows the well-known Snoek's limit [4]: an increase in one of these quantities leads to a decrease in another in such a way that their product remains constant and depends only on a material saturation magnetization. For instance, high-resistivity ferrites have been used in radar and telecommunications systems for more than a half-century, as they are ideal for applications in kHz and MHz range [5]. But the usage of ferrites in the GHz range is extremely limited due to the drastic decrease in magnetic permeability. By using planar magnetic materials, such as thin films and multilayers, it is possible to substantially increase the magnetic permeability and the upper limit of the operating frequency range [6]. The relation between the magnetic permeability and the NFMR frequency introduced by Acher for thin films [3,7] clearly demonstrates the superiority of planar magnetic materials over bulk ones.

From a practical viewpoint, it is important to have a possibility to purposefully synthesize thin films with specific characteristics for microwave applications, first of all, with the specified NFMR frequency. According to the well-known Kittel equation [8], the NFMR frequency of thin films with uniaxial magnetic anisotropy H_k is determined as $f_0 = (\gamma/2\pi)\sqrt{H_k(H_k + 4\pi M_s)}$, where γ is the gyromagnetic ratio, and M_s is the saturation magnetization. Generally, for a specific magnetic

* Corresponding author. Siberian Federal University, 79 Svobodny pr., 660041, Krasnoyarsk, Russia.
** Corresponding author.
E-mail addresses: aizotov@sfu-kras.ru (A.V. Izotov), psolovev@iph.krasn.ru (P.N. Solovev).

https://doi.org/10.1016/j.physb.2021.413654
Received 28 September 2021; Received in revised form 23 December 2021; Accepted 30 December 2021
Available online 3 January 2022

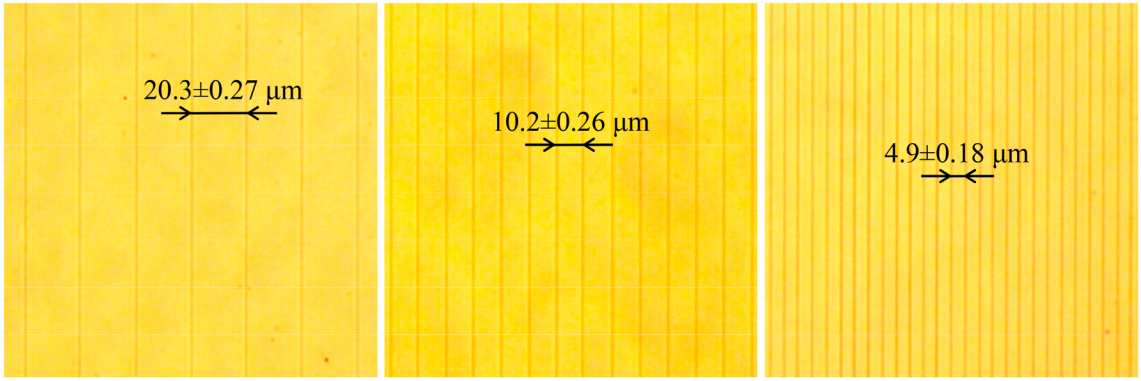

Fig. 1. Surface images of Series 1 films captured with a polarizing optical microscope Axio Imager. A1m (Carl Zeiss).

material, the value of M_s remains practically constant. Hence, the tuning of the resonance frequency f_0 within a wide range can be achieved through the control of the H_k field. A large variety of methods exists that allows one to form a uniaxial magnetic anisotropy in a thin film. For example, uniaxial anisotropy can be induced by an external magnetic field applied either during film deposition [9,10] or during post-deposition thermal annealing [11]. It is also possible to control magnetic anisotropy by the oblique deposition [12–14] and by elastic stresses in case of usage of magnetostrictive materials [15–17].

In recent years, with the advance of nanotechnology, researchers have been actively developing methods for creating thin films with a periodically modulated structure or geometry at micro-to-submicron scales [18–20]. Based on such methods as optical and electron-beam lithography and ion-beam etching, technologies have been developed for producing magnetic structures consisting of individual micro- or nanostripes [21–25], as well as for the fabrication of films with periodically modulated surfaces [26–28]. Thin films with periodic topography were also prepared by the deposition of a magnetic material onto substrates preliminary patterned by the methods of ion-beam erosion [19,29–31], onto thermally annealed sapphire substrates [32–34], and others. These approaches make it possible to controllably adjust in a wide range magnetic anisotropy [21–24,26,29–34] and magnetic permeability [21–23,26,33,34] of such thin-film structures.

In this paper, we explore the capabilities of a fairly simple and universal method for creating periodically patterned thin magnetic films with specified microwave characteristics. This method is based on the fabrication of periodically arranged grooves on the substrate surface by a diamond cutter and the subsequent deposition of a magnetic film onto this patterned substrate. This inexpensive approach allows one to quickly produce large-area films with modulated surfaces and, as shown in this paper, to control the magnetic anisotropy field, NFMR frequency, and damping parameter.

2. Experimental details

To test and study the capabilities of the considered method, two series of samples (Series 1 and 2) were prepared by deposition of Permalloy on micropatterned substrates. We used quartz glass substrates of roughness less than 1 nm and with sizes of $12 \times 12 \times 0.5$ mm^3. Using a specially designed automated coordinatograph, an array of parallel equidistant grooves was made on the surface of these substrates by a diamond cutter. Each series consists of three patterned samples with periods (distance between grooves) of $l = 20$, 10, and 5 μm. But the force exerted by the diamond cutter on the glass surface (the cutting pressure) for Series 1 was 1.5 times smaller than that for Series 2. After the patterning, the standard washing procedure of substrates, including ultrasound treatment, was done.

Thin Permalloy films of thickness 110 nm were deposited on these substrates. Additionally, a reference sample of the same thickness was

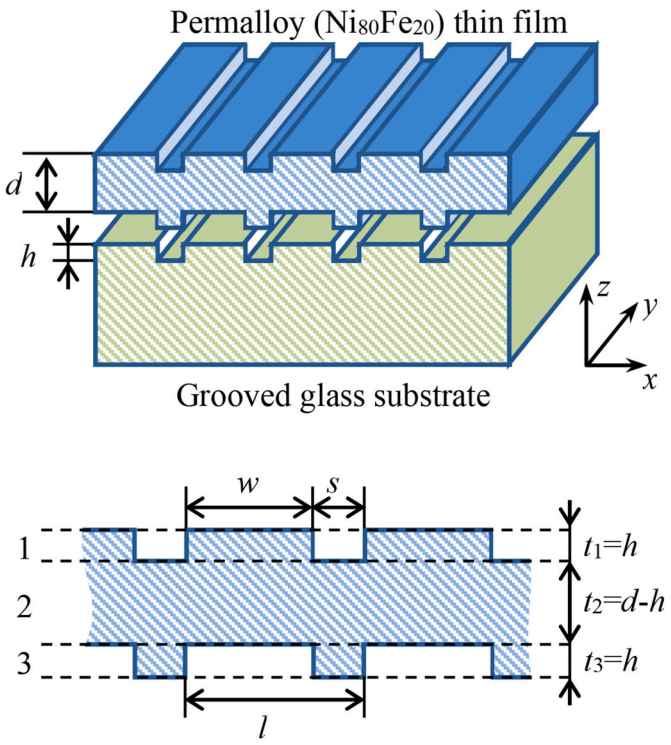

Fig. 2. A model of a thin magnetic film with periodically modulated surfaces.

fabricated by depositing of Permalloy on an unmodified substrate without grooves. All the samples of both series and the reference sample were prepared during one deposition cycle by DC magnetron sputtering of $Fe_{20}Ni_{80}$ wt% target (Kurt J. Lesker Company). The base pressure in the vacuum chamber was 3×10^{-4} Pa, and the sputtering was done at the Ar pressure of 2×10^{-1} Pa. During the deposition, the substrates temperature was kept at 200°C. An in-plane uniform magnetic field of 200 Oe was applied to the depositing films. The samples of Series 1 were oriented such that this field was parallel to the grooves, while for the samples of Series 2 the field was perpendicular to the grooves. The applied field induced a uniaxial magnetic anisotropy H_a with the easy axis (EA) lying along the grooves for the samples of Series 1, and transverse to the grooves for the samples of Series 2.

The thickness and the chemical composition of the prepared samples were controlled using x-ray fluorescence analysis (Pioneer S4, Bruker). The average thickness of the films was 110 ± 2 nm, and the deviation of the films composition from the nominal composition of the target was less than 0.6 wt%. A polarizing optical microscope Axio Imager. A1m (Carl Zeiss) was used to analyze the films pattern. As an example, Fig. 1

shows the images of Series 1 films. It was found that the films surface completely replicates the substrates topography and consists of regularly spaced parallel grooves with width of about 1.5 μm. The measured period of the obtained structures was $l = 20.3 \pm 0.27$, 10.2 ± 0.26, and 4.9 ± 0.18 μm.

Magnetic permeability of the samples was measured using a shorted microstrip line fixture connected to a vector network analyzer (VNA, R&S ZNB20), in the frequency range from 100 MHz to 9.5 GHz. The design of the fixture inside which the investigated sample was placed, and the general scheme of the measurement setup (VNA-FMR spectrometer) were analogous to those described in Ref. [35]. The measurements were carried out in the frequency-sweep mode for various values of an external magnetic field H applied in the sample plane.

3. Theoretical model

For a theoretical analysis of the experimental data, we considered a model of a thin magnetic film with periodically modulated surfaces, as shown in Fig. 2. The magnetic anisotropy of such films can be estimated by using the approach introduced by Netzelmann, which allows one to circumvent the quite complex problem of dipolar interactions in heterogeneous structures. For the analysis of particulate films, Netzelmann [36] represented the demagnetization energy density as a combination of energies of two limiting cases: an isolated particle with the demagnetization tensor N^{obj} and a uniformly magnetized film with the demagnetization tensor N^{film}. By denoting the magnetization vector as **M**, and the packing factor describing the relative fraction of magnetic particles in the sample by p, the dipolar energy density can be expressed as [37–39].

$$F_d = \frac{1}{2}p(1-p)\mathbf{M}N^{obj}\mathbf{M} + \frac{1}{2}p^2\mathbf{M}N^{film}\mathbf{M}. \quad (1)$$

The first term on the right-hand side of equation (1) is the magnetic energy related to the particles shape, and the second term is the demagnetization energy associated with the overall geometry of the sample. In this case, the demagnetization field is determined as

$$\mathbf{H}_d = -\frac{1}{p}\frac{dF_d}{d\mathbf{M}} = -(1-p)N^{obj}\mathbf{M} - pN^{film}\mathbf{M} = -N\mathbf{M}, \quad (2)$$

and the effective demagnetization tensor of a particulate film is $N = (1-p)N^{obj} + pN^{film}$.

In Ref. [37], Dubowik showed that this approach could be applied not only to particulate films but also to other heterogeneous magnetic structures of arbitrary size and shape. In particular, in his work, Dubowik presented examples for the calculation of demagnetization fields for a multilayered film, a film with columnar microstructure, and film with surface roughness. Here, we will use this approach to calculate magnetic anisotropy originated from the periodic steps on the sample surface and at the film/substrate interface, which can be called "substrate-topography-induced magnetic anisotropy". To do this, let us divide the profile of the considered magnetic structure into three layers, as shown in Fig. 2. In this case, the expression for the dipolar energy density, according to Ref. [37], will be

$$F_d = \frac{1}{2}\sum_{i=1}^{3}\frac{t_i}{t}p_i(1-p_i)\mathbf{M}N_i^{obj}\mathbf{M} + \frac{1}{2}\sum_{i=1}^{3}\frac{t_i}{t}p_i^2\mathbf{M}N^{film}\mathbf{M}, \quad (3)$$

where t_i, p_i, and N_i^{obj} are the thickness, density, and demagnetization tensor of isolated "particles" (elongated stripes) of the ith layer, and t is the total thickness of all layers. According to Fig. 2, the thicknesses of individual layers are $t_1 = t_3 = h$, $t_2 = d–h$, and the thickness of the whole structure is $t = d + h$. The densities of individual layers are $p_1 = w/l$, $p_2 = 1$, and $p_3 = s/l$. Let us also denote by $p = (p_1t_1 + p_2t_2 + p_3t_3)/t$ an effective density of the whole structure. Then, the demagnetization field is determined by the expression

$$\mathbf{H}_d = -\frac{1}{p}\frac{dF_d}{d\mathbf{M}} = -\sum_{i=1}^{3}\frac{t_i}{t}\frac{p_i(1-p_i)}{p}N_i^{obj}\mathbf{M} - \sum_{i=1}^{3}\frac{t_i}{t}\frac{p_i^2}{p}N^{film}\mathbf{M} = -N\mathbf{M}, \quad (4)$$

and an effective demagnetization tensor of the three-layer magnetic structure shown in Fig. 2 is

$$N = \sum_{i=1}^{3}\frac{t_i}{t}\frac{p_i(1-p_i)}{p}N_i^{obj} + \sum_{i=1}^{3}\frac{t_i}{t}\frac{p_i^2}{p}N^{film}. \quad (5)$$

In the coordinate system in which the z-axis coincides with the film's normal vector, and x and y axes are oriented transverse and along the stripes respectfully (see Fig. 2), the tensor N^{film} has only one nonzero component $N_{zz}^{film} = 4\pi$. In the experiment, the height of the steps on the film surface was much smaller than their width, that is, $h \ll w$ and $h \ll s$. Therefore, we can use the following approximation for the calculation of the components of the demagnetization tensor N_i^{obj} [40]:

$$N_1^{obj} = 4\pi\begin{bmatrix} t_1/(t_1+w) & 0 & 0 \\ 0 & 0 & 0 \\ 0 & 0 & w/(t_1+w) \end{bmatrix},\ N_2^{obj} = 0,\ N_3^{obj} = 4\pi\begin{bmatrix} t_3/(t_3+s) & 0 & 0 \\ 0 & 0 & 0 \\ 0 & 0 & s/(t_3+s) \end{bmatrix}. \quad (6)$$

The nonzero components of the effective demagnetization tensor (5) will be

$$N_x = N_{xx} = 4\pi\frac{h^2}{dl}\frac{ws}{l}\left[\frac{1}{h+w} + \frac{1}{h+s}\right] \approx 4\pi\frac{h^2}{dl}, N_z = N_{zz} = 4\pi(1-N_{xx}) \approx 4\pi\left(1-\frac{h^2}{dl}\right). \quad (7)$$

Using these expressions, we can write formulas for the calculation of in-plane H_u and perpendicular $4\pi M_{eff}$ magnetic anisotropy fields induced by the demagnetization fields in periodically patterned films

$$H_u = N_xM_s = 4\pi M_s\frac{h^2}{dl},\ 4\pi M_{eff} = N_zM_s = 4\pi M_s\left(1-\frac{h^2}{dl}\right). \quad (8)$$

To compare theoretical and experimental results, we also used the well-known Schlomann expression [41] for the calculation of the demagnetization factor $N_x = N_{xx}$ of a film with periodic surface roughness. By denoting the mean-square deviation for top and bottom surfaces of the film as $<\xi_1^2(x)>$ and $<\xi_3^2(x)>$, according to Ref. [41], $N_x \approx 4\pi^2[<\xi_1^2(x)> + <\xi_3^2(x)>]/dl$. Taking into account the geometry of the film's profile (Fig. 2), and also the approximation $h \ll w$ and $h \ll s$, we obtain

$$H_u = 4\pi M_s\frac{h^2}{dl}\frac{2\pi ws}{l^2},\ 4\pi M_{eff} = 4\pi M_s\left(1-\frac{h^2}{dl}\frac{2\pi ws}{l^2}\right). \quad (9)$$

These expressions for H_u and M_{eff}, based on the Schlomann expression, differ from (8) by an additional factor of $2\pi ws/l^2$. It is easy to show that when $w \approx 4s$ expressions (8) and (9) become equivalent.

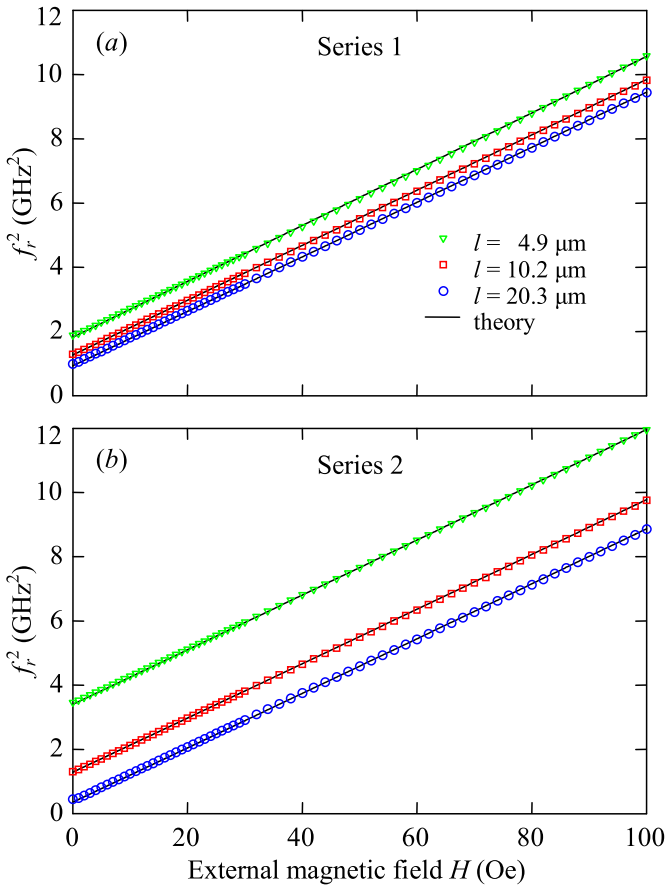

Fig. 3. The FMR frequency squared f_r^2 versus the external field H for the samples of Series 1 (*a*) and Series 2 (*b*).

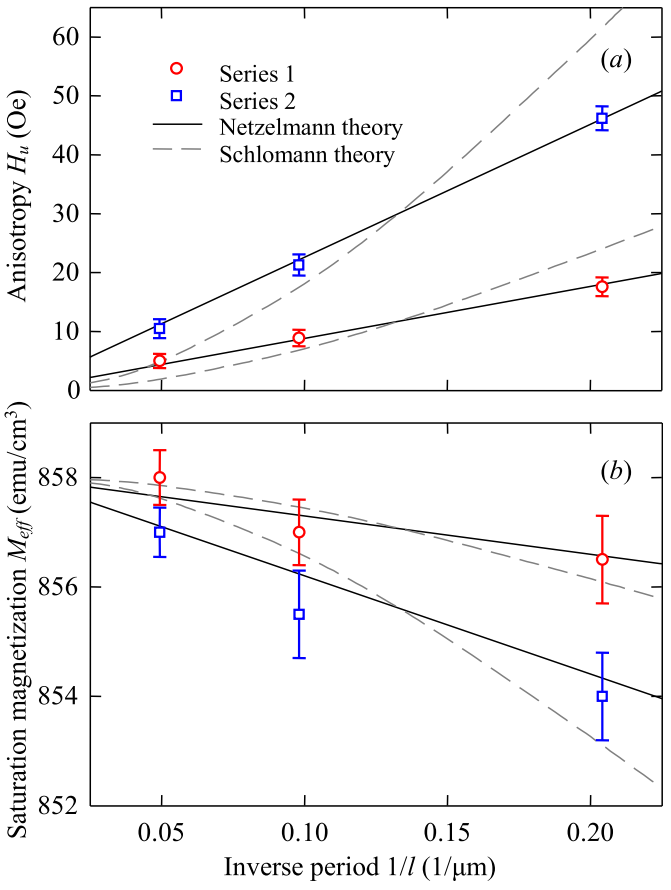

Fig. 4. The dependencies of the topography-induced magnetic anisotropy H_u (*a*) and the effective saturation magnetization M_{eff} (*b*) on the inverse period of grooves. Symbols are the experimental data, solid lines are the calculations using expression (8), and dashed lines are the calculations using (9).

4. Results and discussion

To determine the magnetic parameters of the experimental samples, we measured the dependence of the ferromagnetic resonance (FMR) frequency f_r on the external magnetic field H using the VNA-FMR spectrometer. The field H was applied in the samples plane along the EA and ranged from 0 to 1 kOe. It was found that in patterned films, the direction of EA always coincided with the direction of grooves, that is, the EA was parallel to the *y*-axis (Fig. 2). This indicates that for the samples of Series 2, the field of the magnetic anisotropy H_a induced during deposition was smaller than the field of the substrate-topography-induced magnetic anisotropy H_u originated from the periodic modulations on the films surfaces. In this case, the Kittel equation [8] for the FMR frequency is written as

$$f_r = \frac{\gamma}{2\pi}\sqrt{(H + H_u \pm H_a)(H + H_u \pm H_a + 4\pi M_{eff})}, \quad (10)$$

where the plus sign at H_a refers to the samples of Series 1 ($H_k = H_u + H_a$), and the minus sign to the samples of Series 2 ($H_k = H_u - H_a$). Note that the effective saturation magnetization M_{eff} in (10) is determined by equation (8).

Fig. 3 shows the resonance frequency squared f_r^2 versus applied field H, measured for the samples of Series 1 and 2. Because $4\pi M_{eff} \gg H + H_k$, as follows from equation (10) and can be seen in Fig. 3, the dependence $f_r^2(H)$ is almost linear. Approximating the experimental dependence $f_r(H)$ of the reference sample with $H_u = 0$ and $M_{eff} = M_s$, we first obtained the values of the field-induced anisotropy $H_a = 6$ Oe and the saturation magnetization $M_s = 858$ emu/cm^3. Then, in the same way, we determined H_u and M_{eff} of patterned films. We note that for all samples of Series 1 and 2 when determining H_u, we used the same value of H_a, which was equal to the field-induced anisotropy of the reference sample (6 Oe), because it is not possible to separate experimentally contributions of H_u and H_a to the resulting anisotropy H_k. The solid lines in Fig. 3 show approximating dependencies $f_r^2(H)$ obtained using equation (10).

The symbols in Fig. 4 display experimental values of H_u and M_{eff} plotted as functions of the inverse pattern period 1/l. The theoretical dependencies $H_u(1/l)$ and $M_{eff}(1/l)$ obtained with equation (8) are also shown in the figure, by solid lines. In the calculations, we fitted the value of the groove depth h, which for the Series 1 samples was 30 nm, and 48 nm for Series 2. One can see that the model based on the Netzelmann theory describes well the experimental data and thus can be used in practice for the adjustment of the technology for the fabrication of periodically modulated films with controllable magnetic characteristics. Additionally, the dashed lines in Fig. 4 show results of calculations using expressions (9), obtained on the basis of the Schlomann theory. These theoretical curves are in qualitative agreement with the experimental data, but quantitively they describe experimental values of H_u and M_{eff} worse than the Netzelmann theory.

Tailoring of H_u and M_{eff} by artificially introducing periodic patterns on the substrate also makes it possible to control the NFMR frequency f_0

$$f_0 = \frac{\gamma}{2\pi}\sqrt{(H_u \pm H_a)(H_u \pm H_a + 4\pi M_{eff})}. \quad (11)$$

Fig. 5 (*a*, *b*) and (*c*, *d*) displays frequency spectra of the magnetic permeability $\mu = \mu' - i\mu''$ at zero applied field, obtained using the VNA-FMR spectrometer for the samples of Series 1 and 2, respectfully. The real part of the magnetic permeability μ' describes the dynamic characteristics of a magnetic material, while the imaginary part μ'' characterizes its magnetic losses. As Fig. 5 indicates, below ferromagnetic

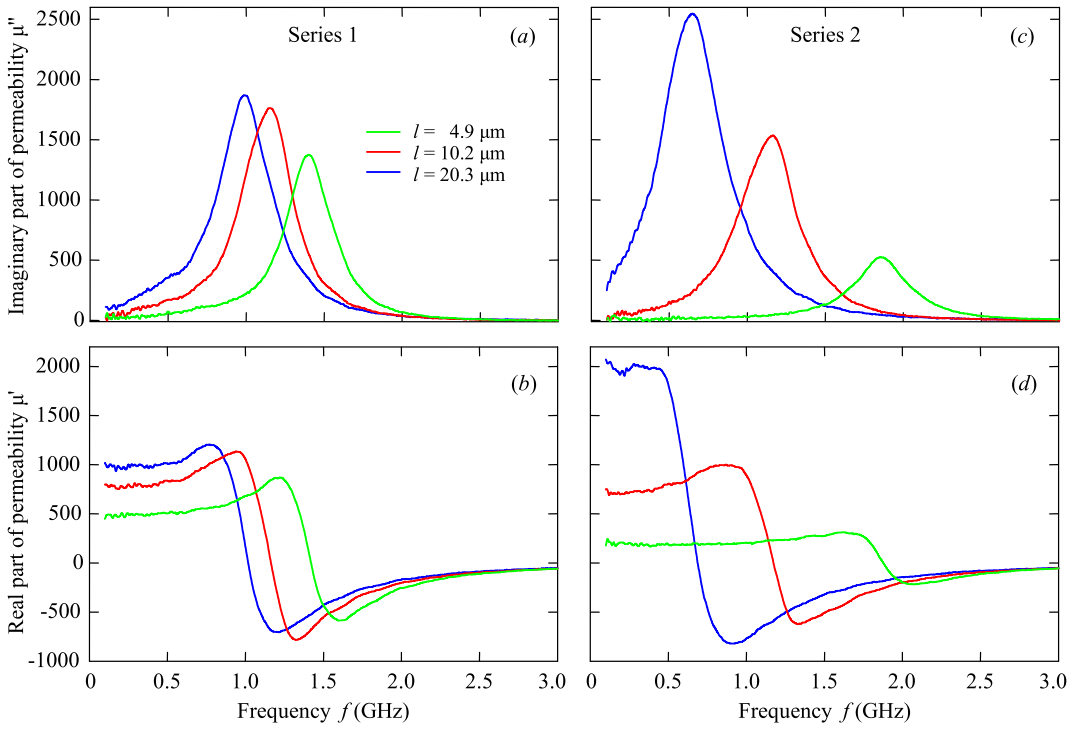

Fig. 5. The frequency dependencies of real and imaginary parts of complex magnetic permeability $\mu = \mu' - i\mu''$ at $H = 0$ for the samples of Series 1 (*a*, *b*) and Series 2 (*c*, *d*).

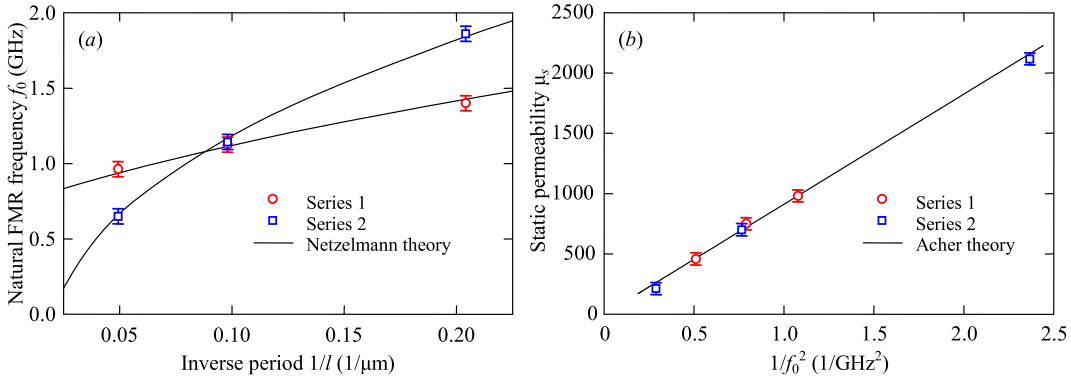

Fig. 6. (*a*) The NFMR frequency f_0 versus the inverse period of grooves. (*b*) The static magnetic permeability μ_s versus the inverse NFMR frequency squared. Symbols are experimental data, and lines are theory.

resonance, the magnetic permeability μ' depends weakly on the frequency and approximately equals to the static magnetic permeability of the material $\mu_s = \mu'(f = 0)$. When the frequency of the excitation signal exceeds the frequency of ferromagnetic resonance, magnetic permeability μ' becomes negative, and with the subsequent increase in frequency tends to unity. Therefore, the NFMR frequency f_0 can be considered as an upper limit of the operating frequency range, within which the magnetic response of material on average is characterized by the static magnetic permeability μ_s.

As can be seen from Fig. 5, with the decrease of the pattern period l and a corresponding increase of the total magnetic anisotropy $H_k = H_u \pm H_a$, the resonance frequency f_0 rises as well. This dependence is shown in Fig. 6*a* by symbols for the experimental samples of both series. The theoretical dependencies $f_0(1/l)$ obtained with (8) and (11) and shown in the figure by solid lines accord well with the experiment. The decrease of the period l from 20 to 5 μm led to an increase in the NFMR frequency by about 1.5 times from 0.96 to 1.40 GHz for the Series 1 samples and almost 3 times from 0.65 to 1.86 GHz for the Series 2 samples.

Also, the increase in f_0 is followed by the decline of the static magnetic permeability (see Fig. 5). This can be explained by considering the Acher's limit [7], according to which the growth of one of these quantities leads to the decrease of another so that the following equality should hold

$$(\mu_s - 1)f_0^2 = (\gamma 4\pi M_s)^2. \tag{12}$$

For soft magnetic thin films $f_0 \ll \gamma 4\pi M_s$, and limit (12) allows for higher values of the static permeability in comparison with the analogous limit $(\mu_s - 1)f_0 = 2/3 \cdot \gamma 4\pi M_s$ introduced by Snoek [4] for bulk materials. Hence, thin magnetic films are the most promising materials for applications where high dynamic magnetic permeability is required. The dependence $\mu_s(1/f_0^2)$ obtained using (12) is shown by the line in Fig. 6*b*, while symbols show the experimental values of the static permeability for the samples of both series. These results indicate that the Acher's limit is valid for films with modulated surfaces as well.

In the context of microwave applications, the effective damping parameter α is one of the key parameters of magnetic films, which

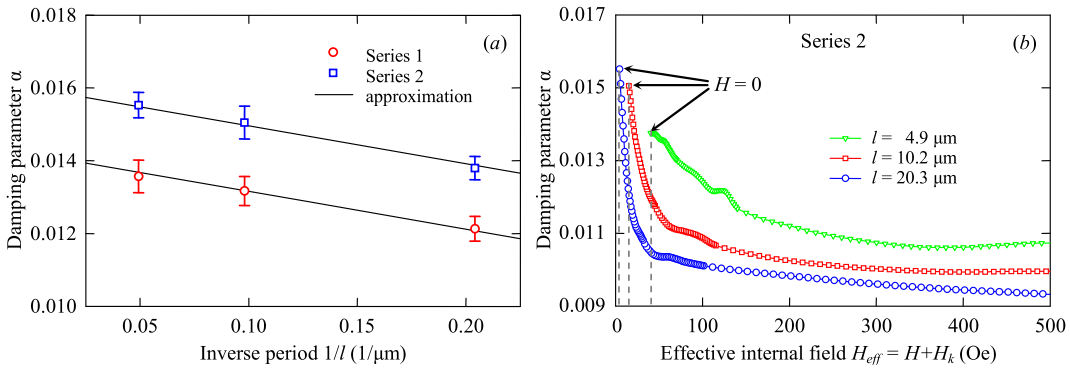

Fig. 7. (*a*) The effective damping parameter versus the inverse period of grooves. The experimental data are symbols, and linear fits are shown by lines. (*b*) The effective damping parameter of Series 2 samples versus an effective internal magnetic field.

characterizes the level of magnetization damping in a magnetic medium [42]. The damping parameter of any magnetic material is primarily determined by the intrinsic mechanisms originated mainly from the interactions between the spins and the electron orbits. However, there also exist another (extrinsic) mechanisms of magnetization relaxation, among which the two-magnon scattering processes give a dominant contribution to the FMR line broadening in thin magnetic films [42,43]. The dimensionless damping parameter α enters the Landau–Lifshitz–Gilbert (LLG) equation of motion as a phenomenological constant and is related to the FMR linewidth Δf as [43].

$$\alpha = \frac{2\pi}{\gamma}\frac{\Delta f}{2(H+H_k)+4\pi M_{eff}}. \tag{13}$$

This relation between the effective damping parameter and FMR linewidth directly follows from the LLG equation and allows one to represent one quantity through another. Using the measured values of the NFMR linewidth (at $H = 0$) for the samples of both series and expression (13), we determined the parameter α (Fig. 7*a*). For both series, the effective damping parameter declines almost linearly with the increase of the inverse period $1/l$. The lines in the figure show the linear fits for the experimental data: $\alpha = -0.0104/l + 0.0142$ for Series 1, and $\alpha = -0.0104/l + 0.016$ for Series 2. These results indicate that the decrease in the grooves period leads to the proportional decrease in the damping for the samples of both series. However, the damping of Series 2 samples, which have deeper grooves, is on average 0.0018 larger than that for the corresponding samples of Series 1 with shallower grooves.

To clarify the cause of α decrease with the decrease of l, in Fig. 7*b* we additionally plot the dependence of the damping parameter on an effective internal magnetic field $H_{eff} = H + H_k$ for the Series 2 samples. As plots demonstrate, the shorter the grooves period l, the higher the overall level of damping in the film. It is expected, since the steps on the film surface and at the film/substrate interface are the source of the nonuniform magnetic fields (magnetic inhomogeneities), which introduce an additional energy dissipation channel through the two-magnon relaxation process [43–45]. Therefore, the higher the steps and the greater their number, the higher the magnitude of magnetic inhomogeneities and correspondingly higher the magnetization damping.

However, we see in Fig. 7*b* that at low effective internal fields damping experiences a sharp increase. This behavior of α is characteristic for all polycrystalline films [46–48], and its main cause is a nonuniform magnetic structure formed in films due to the random distribution of EA in individual crystallites (random magnetic anisotropy) [49,50]. Increasing effective field H_{eff} suppresses the magnetization dispersion leading to the rapid decline and subsequent saturation of the damping parameter [49,50]. As Fig. 7*b* suggests, at low values of H_{eff}, the random anisotropy affects damping much stronger than the artificial surface modulations. Since the effective internal magnetic field under NFMR conditions at $H = 0$ (marked by arrows in Fig. 7*b*) is higher for the films with shorter grooves period, we observe the decrease of damping with the decrease of l in Fig. 7*a*.

5. Conclusion

In this paper, we have investigated thin magnetic films 110 nm in thickness produced by the deposition of Permalloy on grooved substrates. The periodic grooves, with a period ranging from 5 to 20 μm, was formed on the substrate surface by a diamond cutter using a specially designed automated coordinatograph. We have revealed a strong dependence of the magnetic anisotropy, magnetic permeability, and the NFMR frequency and linewidth on the grooves period l. Particularly, it was found that with the decrease of period l, the substrate-topography-induced magnetic anisotropy H_u rises as $\sim 1/l$ and the NFMR frequency increases as $\sqrt{H_u}$. Also, the NFMR linewidth exhibited a noticeable decline with the shortening of period l. It was suggested that the increase in the effective internal magnetic field with the decrease of l results in the suppression of the nonuniform magnetic structure, which emerges in polycrystalline films due to the random distribution of EA in individual crystallites. This, in turn, leads to the decrease of the magnetization damping. We have considered a theoretical model of a thin magnetic film with periodical steps on its surface and at the film/substrate interface. Based on this model, in the framework of the Netzelmann theory, we have obtained expressions for the calculation of the in-plane and perpendicular magnetic anisotropy of such patterned films, which allowed us to explain experimental results.

In conclusion, we note that the technique for producing films with periodically modulated surfaces used in this work is simple and inexpensive. And, considering close agreement between theory and experiment, this approach has a high potential for usage in practice for the design and fabrication of thin films with controllable microwave characteristics.

Credit author statement

A. V. Izotov: Conceptualization, Methodology, Software, Writing - original draft, Supervision. B. A. Belyaev: Conceptualization, Supervision, Writing - review & editing, Funding acquisition. N. M. Boev: Software, Visualization. A. V. Burmitskikh: Investigation, Methodology. A. A. Leksikov: Investigation, Methodology. G. V. Skomorokhov: Investigation, Visualization. P. N. Solovev: Conceptualization, Methodology, Writing - original draft.

Declaration of competing interest

The authors declare that they have no known competing financial interests or personal relationships that could have appeared to influence the work reported in this paper.

Acknowledgments

This work was supported by the Ministry of Science and Higher Education of the Russian Federation, agreement number 075-11-2019-054 dated November 22, 2019.

References

[1] J.G. Andrews, S. Buzzi, W. Choi, S.V. Hanly, A. Lozano, A.C.K. Soong, J.C. Zhang, What will 5G be? IEEE J. Sel. Area. Commun. 32 (2014) 1065–1082, https://doi.org/10.1109/JSAC.2014.2328098.
[2] O. Acher, Modern microwave magnetic materials: recent advances and trends, J. Magn. Magn Mater. 321 (2009) 2033–2034, https://doi.org/10.1016/j.jmmm.2008.09.021.
[3] A.N. Lagarkov, K.N. Rozanov, High-frequency behavior of magnetic composites, J. Magn. Magn Mater. 321 (2009) 2082–2092, https://doi.org/10.1016/j.jmmm.2008.08.099.
[4] Snoek J C Dispersion and Absorption in Magnetic Ferrites at Frequencies above One Mc/s 1948 *Physica* **XIV** 207–217 (doi: 10.1016/0031-8914(48)90038-X).
[5] V.G. Harris, Microwave Magnetic Materials *Handbook Of Magnetic Materials*, vol. 20, Elsevier B.V, North-holland, 2012, pp. 1–63, https://doi.org/10.1016/B978-0-444-56371-2.00001-5.
[6] I.T. Iakubov, A.N. Lagarkov, S.A. Maklakov, A.V. Osipov, K.N. Rozanov, I. A. Ryzhikov, V.V. Samsonova, A.O. Sboychakov, Microwave and static magnetic properties of multi-layered iron-based films, J. Magn. Magn Mater. 321 (2009) 726–729, https://doi.org/10.1016/j.jmmm.2008.11.036.
[7] O. Acher, A.L. Adenot, Bounds on the dynamic properties of magnetic materials, Phys. Rev. B 62 (2000) 11324–11327, https://doi.org/10.1103/PhysRevB.62.11324.
[8] C. Kittel, On the theory of ferromagnetic resonance absorption, Phys. Rev. 73 (1948) 155–161, https://doi.org/10.1103/PhysRev.73.155.
[9] Y. Fu, I. Barsukov, R. Meckenstock, J. Lindner, H. Raanaei, B. Hjorvarsson, M. Farle, Mechanism of tailored magnetic anisotropy in amorphous Co68Fe24Zr8 thin films, Appl. Phys. Lett. 104 (2014), 072409, https://doi.org/10.1063/1.4865369.
[10] B.A. Belyaev, A.V. Izotov, S.Y. Kiparisov, G.V. Skomorokhov, Synthesis and study of the magnetic characteristics of nanocrystalline cobalt films, Phys. Solid State 50 (2008) 676–683, https://doi.org/10.1134/S1063783408040136.
[11] Y. Yang, B. Liu, D. Tang, B. Zhang, M. Lu, H. Lu, Influence of the magnetic field annealing on the extrinsic damping of FeCoB soft magnetic films, J. Appl. Phys. 108 (2010), 073902, https://doi.org/10.1063/1.3489954.
[12] X. Zhu, Z. Wang, Y. Zhang, L. Xi, J. Wang, Q. Liu, Tunable resonance frequency of FeNi films by oblique sputtering, J. Magn. Magn Mater. 324 (2012) 2899–2901, https://doi.org/10.1016/j.jmmm.2012.04.035.
[13] B.A. Belyaev, A.V. Izotov, P.N. Solovev, Competing magnetic anisotropies in obliquely deposited thin permalloy film, Phys. B Condens. Matter 481 (2016) 86–90, https://doi.org/10.1016/j.physb.2015.10.036.
[14] P. Solovev, A. Izotov, B. Belyaev, Microstructural and magnetic properties of thin obliquely deposited films: a simulation approach, J. Magn. Magn Mater. 429 (2017) 45–51, https://doi.org/10.1016/j.jmmm.2017.01.012.
[15] Z.K. Wang, E.X. Feng, Q.F. Liu, J.B. Wang, D.S. Xue, Tuning stress-induced magnetic anisotropy and high frequency properties of FeCo films deposited on different curvature substrates, Physica B 407 (2012) 3872–3875, https://doi.org/10.1016/j.physb.2012.06.012.
[16] B.A. Belyaev, A.V. Izotov, Ferromagnetic resonance study of the effect of elastic stresses on the anisotropy of magnetic films, Phys. Solid State 49 (2007) 1731–1739, https://doi.org/10.1134/S106378340709020X.
[17] B.A. Belyaev, A.V. Izotov, P.N. Solovev, N.M. Boev, Strain-gradient-induced unidirectional magnetic anisotropy in nanocrystalline thin permalloy films, Phys. Status Solidi RRL 14 (2019) 1900467, https://doi.org/10.1002/pssr.201900467.
[18] J.W. Lau, J.M. Shaw, Magnetic nanostructures for advanced technologies: fabrication, metrology and challenges, J. Phys. D Appl. Phys. 44 (2011) 303001, https://doi.org/10.1088/0022-3727/44/30/303001.
[19] J. Fassbender, T. Strache, M.O. Liedke, D. Markó, S. Wintz, K. Lenz, A. Keller, S. Facsko, I. Mönch, J. McCord, Introducing artificial length scales to tailor magnetic properties, New J. Phys. 11 (2009) 125002, https://doi.org/10.1088/1367-2630/11/12/125002.
[20] A.O. Adeyeye, J. Singh, Large area patterned magnetic nanostructures, J. Phys. D Appl. Phys. 41 (2008) 153001, https://doi.org/10.1088/0022-3727/41/15/153001.
[21] Y. Ren, X. Li, Y. Wang, J. Ren, Y. Zhang, B. Dai, H. Yan, G. Sun, S. Peng, Patterned FeNi soft magnetic strips film with tunable resonance frequency from 1 to 10.6 GHz, Sci. Rep. 6 (2016) 31773, https://doi.org/10.1038/srep31773.
[22] X. Chen, Y.G. Ma, C.K. Ong, Magnetic anisotropy and resonance frequency of patterned soft magnetic strips, J. Appl. Phys. 104 (2008), 013921, https://doi.org/10.1063/1.2953065.
[23] Z. Zhu, H. Feng, X. Cheng, H. Xie, Q. Liu, J. Wang, Static and dynamic magnetic properties of stripe-patterned Fe20Ni80 soft magnetic films, J. Phys. D Appl. Phys. 51 (2018), 045004, https://doi.org/10.1088/1361-6463/aa9dfa.
[24] M. Belmeguenai, M.S. Gabor, F. Zighem, D. Berling, Y. Roussigné, T. Petrisor, S. M. Chérif, C. Tiusan, O. Brinza, P. Moch, Static and dynamic magnetic properties of Co2FeAl-based stripe arrays, J. Magn. Magn Mater. 399 (2016) 199–206, https://doi.org/10.1016/j.jmmm.2015.09.065.
[25] Z.K. Wang, V.L. Zhang, H.S. Lim, S.C. Ng, M.H. Kuok, S. Jain, A.O. Adeyeye, Nanostructured magnonic crystals with size-tunable bandgaps, ACS Nano 4 (2010) 643–648, https://doi.org/10.1021/nn901171u.
[26] L. Pan, H. Xie, X. Cheng, C. Zhao, H. Feng, D. Cao, J. Wang, Q. Liu, Tuning the ferromagnetic resonance frequency of soft magnetic film by patterned permalloy micro-stripes with stripe-domain, J. Magn. Mater. 457 (2018) 46–51, https://doi.org/10.1016/j.jmmm.2018.02.060.
[27] M. Langer, R.A. Gallardo, T. Schneider, S. Stienen, A. RoldanMolina, Y. Yuan, K. Lenz, J. Lindner, P. Landeros, J. Fassbender, Spin-wave modes in transition from a thin film to a full magnonic crystal, Phys. Rev. B 99 (2019), 024426, https://doi.org/10.1103/PhysRevB.99.024426.
[28] G.N. Kakazei, X.M. Liu, J. Ding, A.O. Adeyeye, Ni80Fe20 film with periodically modulated thickness as a reconfigurable one-dimensional magnonic crystal, Appl. Phys. Lett. 104 (2014), 042403, https://doi.org/10.1063/1.4863508.
[29] S.K. Vayalil, A. Koorikkat, A.K. Gopi, S.V. Roth, P.S.A. Kumar, Tailoring of uniaxial magnetic anisotropy in Permalloy thin films using nanorippled Si substrates, J. Phys. Condens. Matter 32 (2020) 185804, https://doi.org/10.1088/1361-648X/ab6d0d.
[30] K. Bukharia, P. Karmakar, D. Kumar, V.R. Reddy, A. Gupta, Evolution of magnetic anisotropy in cobalt film on nanopatterned silicon substrate studied in situ using MOKE, J. Magn. Magn Mater. 497 (2020) 165934, https://doi.org/10.1016/j.jmmm.2019.165934.
[31] M.O. Liedke, M. Körner, K. Lenz, M. Fritzsche, M. Ranjan, A. Keller, E. Čižmár, S. A. Zvyagin, S. Facsko, K. Potzger, J. Lindner, J. Fassbender, Crossover in the surface anisotropy contributions of ferromagnetic films on rippled Si surfaces, Phys. Rev. B 87 (2013), 024424.
[32] S. Ki, J. Dho, Strong uniaxial magnetic anisotropy in triangular wave-like ferromagnetic NiFe thin films, Appl. Phys. Lett. 106 (2015) 212404, https://doi.org/10.1063/1.4921784.
[33] Y. Zhang, Y. Ren, J. Lv, R. Zhou, B. Dai, Tunable high-frequency magnetic properties of NiFe films on triangular wave-like surface of Al2O3 substrate, Chem. Phys. Lett. 749 (2020) 137411, https://doi.org/10.1016/j.cplett.2020.137411.
[34] X. Xu, L. Jin, T. Wen, Y. Liao, X. Tang, H. Zhang, Z. Zhong, Effects of substrate annealing on uniaxial magnetic anisotropy and ferromagnetic resonance frequency of Ni80Fe20 films deposited on self-organized periodically rippled sapphire substrates, Vacuum (2021) **186** 110047, https://doi.org/10.1016/j.vacuum.2021.110047.
[35] J. Wei, J. Wang, Q. Liu, X. Li, D. Cao, X. Sun, An induction method to calculate the complex permeability of soft magnetic films without a reference sample, Rev. Sci. Instrum. 85 (2014), 054705, https://doi.org/10.1063/1.4876598.
[36] Netzelmann U 1990 Ferromagnetic resonance of particulate magnetic recording tapes J. Appl. Phys. 68 1800–1807 (doi: 10.1063/1.346613).
[37] Dubowik J 1996 Shape anisotropy of magnetic heterostructures Phys. Rev. B 54 1088–1091 (doi: 10.1103/PhysRevB.54.1088).
[38] J. Dubowik, Erratum: shape anisotropy of magnetic heterostructures, Phys. Rev. B 54 (2000) 1088, https://doi.org/10.1103/PhysRevB.62.727. Phys. Rev. B 62 727, 1996.
[39] G.N. Kakazei, A.F. Kravets, N.A. Lesnik, M.M. Pereira de Azevedo, G. Pogorelov Yu, J.B. Sousa, Ferromagnetic resonance in granular thin films, J. Appl. Phys. 85 (1999) 5654–5656, https://doi.org/10.1063/1.369830.
[40] R.I. Joseph, E. Schlömann, Demagnetizing field in nonellipsoidal bodies, J. Appl. Phys. 36 (1965) 1579–1593, https://doi.org/10.1063/1.1703091.
[41] E. Schlomann, Demagnetizing fields in thin magnetic films due to surface roughness, *J. Appl.* Phys. 41 (1970) 1617–1622, https://doi.org/10.1063/1.1659081.
[42] A. Barman, J. Sinha, Spin Dynamics and Damping in Ferromagnetic Thin Films and Nanostructures, Springer International Publishing AG, Switzerland), 2018.
[43] A.G. Gurevich, G.A. Melkov, Magnetization Oscillations and Waves, CRC Press, Boca Raton, FL, 1996.
[44] R. Arias, D.L. Mills, Extrinsic contributions to the ferromagnetic resonance response of ultrathin films, Phys. Rev. B 60 (1999) 7395–7409, https://doi.org/10.1103/PhysRevB.60.7395.
[45] R.D. McMichael, P. Krivosik, Classical model of extrinsic ferromagnetic resonance linewidth in ultrathin films, IEEE Trans. Magn. 40 (2004) 2–11, https://doi.org/10.1109/TMAG.2003.821564.
[46] M.L. Schneider, T. Gerrits, A.B. Kos, T.J. Silva, Experimental determination of the inhomogeneous contribution to linewidth in Permalloy films using a time-resolved magneto-optic Kerr effect microprobe, J. Appl. Phys. 102 (2007), 053910, https://doi.org/10.1063/1.2772563.
[47] C.B. Craus, A.R. Chezan, D.O. Boerma, L. Niesen, Magnetization dynamics of soft nanocrystalline thin films with random magnetocrystalline anisotropy and induced uniaxial anisotropy, J. Phys. Condens. Matter 16 (2004) 9227–9241, https://doi.org/10.1088/0953-8984/16/50/013.
[48] T.-J. Hwang, J. Lee, K.H. Kim, D.H. Kim, Magnetic properties and high frequency characteristics of FeCoN thin films, AIP Adv. 6 (2016), 055914, https://doi.org/10.1063/1.4943358.
[49] A.V. Izotov, B.A. Belyaev, P.N. Solovev, N.M. Boev, Grain-size dependence of magnetic microstructure and high-frequency susceptibility of nanocrystalline thin films: a micromagnetic simulation study, J. Magn. Magn Mater. 529 (2021) 167856, https://doi.org/10.1016/j.jmmm.2021.167856.
[50] B.A. Belyaev, N.M. Boev, A.V. Izotov, P.N. Solovev, Study of peculiarities of the microwave absorption spectrum of nanocrystalline thin magnetic films, Russ. Phys. J. 61 (2019) 1798–1805, https://doi.org/10.1007/s11182-019-01603-4.